

Article

# Degradation Behavior, Transport Mechanism and Osteogenic Activity of Mg–Zn–RE Alloy Membranes in Critical-Sized Rat Calvarial Defects

Mingyu Zhao <sup>1,2,†</sup>, Guanqi Liu <sup>1,3,4,†</sup>, Ying Li <sup>1,3,4</sup>, Xiaodong Yu <sup>3,4</sup>, Shenpo Yuan <sup>1</sup>, Zhihua Nie <sup>3</sup> , Jiewen Wang <sup>3</sup>, Jianmin Han <sup>1,\*</sup>, Chengwen Tan <sup>3,4,\*</sup> and Chuanbin Guo <sup>2,\*</sup>

<sup>1</sup> National Engineering Laboratory for Digital and Material Technology of Stomatology, Department of Dental Materials, Peking University School and Hospital of Stomatology, Beijing 100081, China; zhaomy2014@163.com (M.Z.); 18811321319@163.com (G.L.); lilyxiaohuochai@foxmail.com (Y.L.); yuanshenpo@163.com (S.Y.)

<sup>2</sup> Department of Oral and Maxillofacial Surgery, Peking University School and Hospital of Stomatology, Beijing 100081, China

<sup>3</sup> School of Materials Science and Engineering, Beijing Institute of Technology, Beijing 100081, China; yuxiaodong.bit@163.com (X.Y.); znie@bit.edu.cn (Z.N.); jwwang2015@foxmail.com (J.W.)

<sup>4</sup> China Astronaut Res & Training Ctr, Beijing 100081, China

\* Correspondence: hanjianmin@bjmu.edu.cn (J.H.); tanchengwen@126.com (C.T.); guodazuo@vip.sina.com (C.G.); Tel.: +86-10-82195746 (J.H.); +86-10-68912712 (C.T.); +86-10-82195748 (C.G.)

† These authors contributed equally to this work.

Received: 22 April 2020; Accepted: 18 May 2020; Published: 22 May 2020



**Abstract:** In this study, a specific Mg–Zn–RE alloy membrane with 6 wt.% zinc and 2.7 wt.% rare earth elements (Y, Gd, La and Ce) was prepared to investigate implant degradation, transport mechanism and guide bone regeneration in vivo. The Mg-membrane microstructure and precipitates were characterized by the scanning electron microscopy (SEM) and the transmission electron microscopy (TEM). The Mg-membrane degradation process and effect on osteogenesis were investigated in a critical-sized rat calvarial defect model via micro-CT examination and hard tissue slicing after 2-, 5- and 8-week implants. Then, the distribution of elements in organs after 1-, 2- and 4-weeks implantation was examined to explore their transportation routes. Results showed that two types of precipitates had formed in the Mg-membrane after a 10-h heat treatment at 175 °C:  $\gamma$ -phase MgZn precipitation with dissolved La, Ce and Gd, and W-phase  $Mg_3(Y, Gd)_2Zn_3$  precipitation rich in Y and Gd. In the degradation process of the Mg-membrane, the Mg matrix degraded first, and the rare earth-rich precipitation particles were transferred to a more stable phosphate compound. The element release rate was dependent on the precipitate type and composition. Rare earth elements may be transported mainly through the lymph system. The defects were repaired rapidly by the membranes. The Mg-membrane used in the present study showed excellent biocompatibility and enhanced bone formation in the vicinity of the implants.

**Keywords:** magnesium alloy; rare earth elements; precipitate; in vivo degradation; transport mechanism; osteogenic activity

## 1. Introduction

In recent years, magnesium (Mg)-based alloys have become a special focus for medical applications, due to their excellent biomechanical properties and biodegradability [1]. Compared with other biomedical metals, the densities of Mg-based alloys are closer to that of human natural bone, and their elastic modulus are more similar to that of natural bone, thus avoiding “stress shielding” effect caused

by mismatch of elastic modulus between implants and human bone tissues [2–4]. Mg-based alloys are degradable in the physiological environment, which do not need to be removed by the secondary surgery after healing, reducing many risks of patients [5–7]. In addition, Mg-based alloys have been shown to have stimulatory effects on the growth of adjacent new bone tissues [8,9]. Therefore, Mg-based alloys show promise for orthopedic and dental applications, and can be applied in various ways, e.g., as screws, plates or other fixture devices [10]. There are specific properties requirements for each intended use. Various Mg-based alloys have been tailored to optimize degradation behavior and other properties by using appropriate alloying elements, surface modification, coating, thermal treatment, and so on. Rare earth elements (REEs) are often added to Mg-based alloys to regulate corrosion rate [11–15] and mechanical properties [16]. To date, several Mg–RE alloy implants have been used successfully in in vivo applications, such as WE43 [17], ZEK100 [18] and LAE442 [19]. However, the alloy elements will be released over time due to degradation of the implanted alloy, which could induce toxic reactions depending on the locally released element concentration and/or systemic accumulation. It is well known that most REEs have moderate to severe toxicity and the REEs released from Mg–RE alloys pose a potential risk. However, there is still a lack of knowledge regarding the potential effects of REEs and their clearance from the body in vivo.

REEs are defined as a group of 17 elements [13], usually added as a mischmetal of various compositions commonly rich in Ce, La, Gd and Y. REEs can exist as a solid solution or precipitate in Mg alloys. Within an Mg matrix, REEs show varying solubility and form various types of precipitates. Therefore, the rates of degradation and release of REEs are not only spatially inhomogeneous, but also temporally nonuniform. Studying the degradation process of REEs is necessary to clarify their biologic action. Some short-term experiments in vitro revealed that REEs can form corresponding oxide barrier layers on Mg alloy surfaces [14,20]. For example, Y element in Mg alloys causes the formation of  $Y_2O_3$  in simulated body fluid (SBF) [12] and also in Hank's solution at 37 °C [21]. However, there are few studies concerning the degradation process of REEs in Mg in vivo. In addition, although a number of different Mg–RE alloys have been tested [22,23], few studies have observed degradation throughout the entire degradation period [23,24]. This current deficiency within Mg–RE alloy research may be due to previously studied implants taking a long time to degrade because of their size, shape and site location. For example, cylindrical-shaped implants with a diameter of 1.6–2.5 mm inserted into tibia and femur bones will take a long time to completely degrade [23,24]. In vivo studies on the distribution and accumulation of REEs in some Mg–RE alloys have been performed [25,26], but the transportation mechanisms of REEs within organs remain poorly understood. Nevertheless, such studies are crucially important for exploring novel materials.

Among Mg alloys, Mg–6Zn alloys have appropriate mechanical properties and are believed to be good candidates for implant applications [27,28]. Therefore, in this study, Mg–6Zn was used as the base alloy with 2.7 wt.% REEs (Y, Gd, La and Ce), denoted by Mg–6Zn–2.7RE. Y and Gd mainly formed a second phase, and La and Ce were mainly present in solid solution. In this study, it was possible to examine the degradation of REEs in both the second phase and the solid solution. The Mg–6Zn–2.7RE was prepared as a membrane, which can degrade rapidly. This is convenient to study the degradation pathways of various elements in a relatively short time.

## 2. Materials and Methods

### 2.1. Sample Preparation

The wrought Mg–6Zn–2.7RE alloy contains 0.90 wt.% Gd, 0.75 wt.% Y, 0.96 wt.% Ce and 0.08 wt.% La, which was provided by AECC Beijing Institute of Aeronautical Materials. The alloy was heated at 410 °C for 10 h followed by air cooling, then aged at 175 °C for 10 h. Membranes with a diameter of 5 mm were cut to 130 µm thickness by mechanical wire cutting and then ground with 2000 grit silicon carbide (SiC) paper to 110 µm thickness. Subsequently, all samples were treated by ultrasonic

cleaning in acetone and ethanol. The samples were sterilized with ultraviolet irradiation (UV lamp, predominantly 254 nm) for 30 min before being inserted into the rats.

## 2.2. Characteristics of Precipitates

The components and distribution of the precipitates were characterized using a field emission scanning electron microscope (SEM, QUANTA 200F, FEI, Hillsboro, OR, USA) in back-scattered electron mode with an energy dispersive spectrometer (EDS) and transmission electron microscope (TEM, Tecnai G2 F20; FEI, Hillsboro, OR, USA). In preparation for the SEM analysis, samples were mounted, ground with SiC paper and polished with diamond paste down to a 0.5  $\mu\text{m}$  finish. In addition, the samples for SEM analysis were lightly etched with 10 vol.% nitric acid in methanol. The thin foils for TEM analysis were cut perpendicular to the extrusion direction, punched into discs with a diameter of 3 mm, mechanically ground to 50  $\mu\text{m}$  in thickness, and then ion milled.

## 2.3. Degradation and Histological Evaluation In Vivo

### 2.3.1. Surgical Procedure

Forty-four 8-week-old Sprague-Dawley (SD) rats were used in this study. The study protocol was approved by the Animal Care and Use Committee of Peking University. The animals were anesthetized by intraperitoneal injection of pentobarbital sodium (50 mg/kg body weight). Hair on the cranial bone was removed by shaving, and the exposed area was wiped by swabbing with 3 vol.% povidone-iodine followed by 75 vol.% ethanol for disinfection. We incised the skin, subcutaneous tissue and periosteum along the midline, and exposed the bone via blunt dissection. Two 6-mm-sized full thickness bone defects were prepared on both sides of the midline of the parietal bone using a saline-cooled trephine drill. Each defect was washed with saline to remove bone debris. The Mg-6Zn-2.7RE alloy membranes were inserted into the defects (Figure 1). Finally, the tissues were sutured in layers.

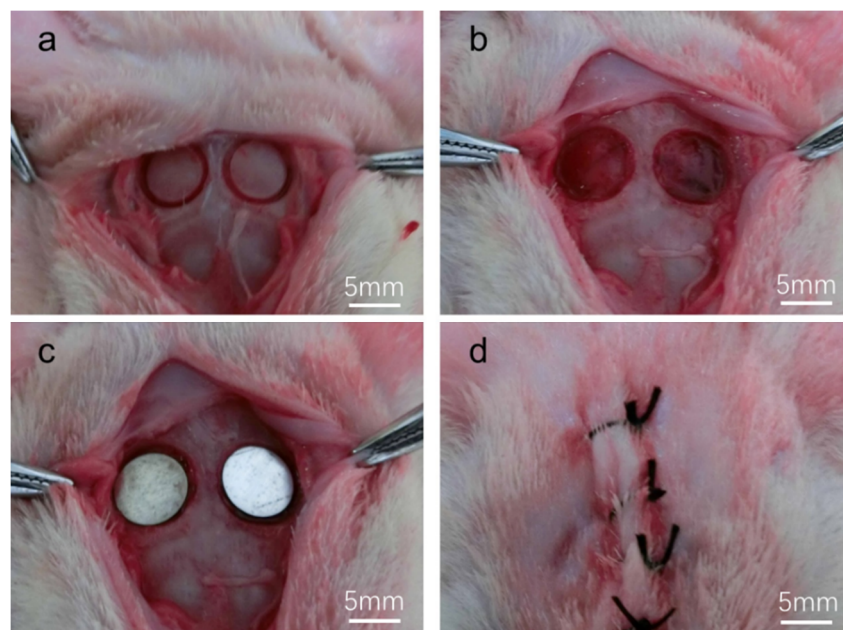


**Figure 1.** Implant placement into calvarial bone defects. (a) Incising the skin, subcutaneous tissue and periosteum along the midline and exposing the bone via blunt dissection; (b) two 6-mm-size full-thickness bone defects created on both sides of the midline of the parietal bone using a saline-cooled trephine drill. Each defect was washed with saline to remove bone debris; (c) Mg-6Zn-2.7RE alloy membranes inserted into the defects; (d) suturing of the wound.

After 2, 5 and 8-week healing periods, eight SD rats per healing period were euthanized, and the implant specimens were harvested with surrounding bone tissue. The tissue specimens were fixed in 90 vol.% ethanol solution. Five SD rats per healing period (1, 2 and 4 weeks) and five SD rats without any surgical treatment (as a blank control group) were euthanized, and the organs (brain, heart, liver, spleen, lung, kidney, adrenal gland, submandibular lymph nodes) of each animal were collected and frozen immediately at  $-80\text{ }^{\circ}\text{C}$ . The organs were harvested and handled using Teflon-coated tweezers and ceramic scissors which were disinfected by 75% ethanol to avoid possible contamination.

### 2.3.2. Radiographic Evaluation (Microcomputed Tomography (Micro-CT) Analyses)

To evaluate the volumes of alloy materials remaining after degradation and the new bone formation, micro-CT was performed using an Inveon MM system (Siemens, Munich, Germany). Images were acquired at an effective pixel size of  $8.82\text{ }\mu\text{m}$ , voltage of 80 kV, current of  $500\text{ }\mu\text{A}$  and exposure time of 1500 ms in each of the  $360^{\circ}$  rotational steps. The volumes of remaining materials and new bone formation were calculated using Inveon Research Workplace software (Siemens, Knoxville, TN, USA).

### 2.3.3. Histological Processing

The samples were dehydrated in an ascending series of alcohol concentrations (50, 60, 70, 80, 90 and 99 vol.%) and finally embedded in autopolymerizing methyl methacrylate (MMA) resin (Wako Pure Chemical Industries, Ltd., Tokyo, Japan). The non-decalcified specimens ( $300\text{ }\mu\text{m}$  thickness) were cut using a diamond saw (STX-202A, Shenyang Kejing Auto-Instrument Co., Ltd., Shenyang, China), adhered to the resin slides, and successively ground to a thickness of about  $50\text{ }\mu\text{m}$ . Then the ground specimens were stained with methylene blue trihydrate and van Gieson stain. The images were taken under a light microscope. The histological evaluation mainly focused on indicators of inflammation, new bone formation, degradation of alloy materials and the response of surrounding tissues to the implant materials.

### 2.3.4. Degradation Characterization In Vivo (SEM Examination)

After embedding in MMA resin, the samples were cut using a diamond saw (STX-202A, Shenyang Kejing Auto-Instrument Co., Ltd., Shenyang, China) to expose the implant and bone and then cut using an automated microtome (RM 2255; Leica, Wetzlar, Germany) to obtain a smooth and fresh surface. The samples for SEM were carbon (C)-coated using an Auto Fine Coater (JFC-1600; JEOL, Ltd., Tokyo, Japan). The surface morphology was observed with a Quanta 200 field emission gun (FEG) SEM (FEI) in backscattered electron mode. The composition of the degradation products was analyzed by an EDS.

### 2.3.5. Determination of REEs, Mg and Zn in Organs

The organ samples were weighed accurately and placed in a 50 mL Erlenmeyer flask. The samples were digested with 10 mL of mixed acid (nitric acid: perchloric acid in a 9:1 ratio) in a microwave system. Then, the mixed acid was replaced by ultrapure water. The concentrations of Mg, Zn, Gd, Y and La were measured by inductively coupled plasma mass spectrometry (ICP-MS; Thermo Scientific, Waltham, MA, USA). The single element standards of Mg ( $10,000\text{ mg/L}$ , in 2%  $\text{HNO}_3$ ) and Zn ( $10,000\text{ mg/L}$ , in 2%  $\text{HNO}_3$ ) were purchased from China Metrology Science Research. The single element standards of REEs (Gd, Y and La) ( $100\text{ }\mu\text{g/mL}$ , in 2%  $\text{HNO}_3$ ) were purchased from the National Nonferrous Metals and Electronic Materials Analysis and Testing Center (Beijing, China).

### 2.3.6. Statistical Analysis

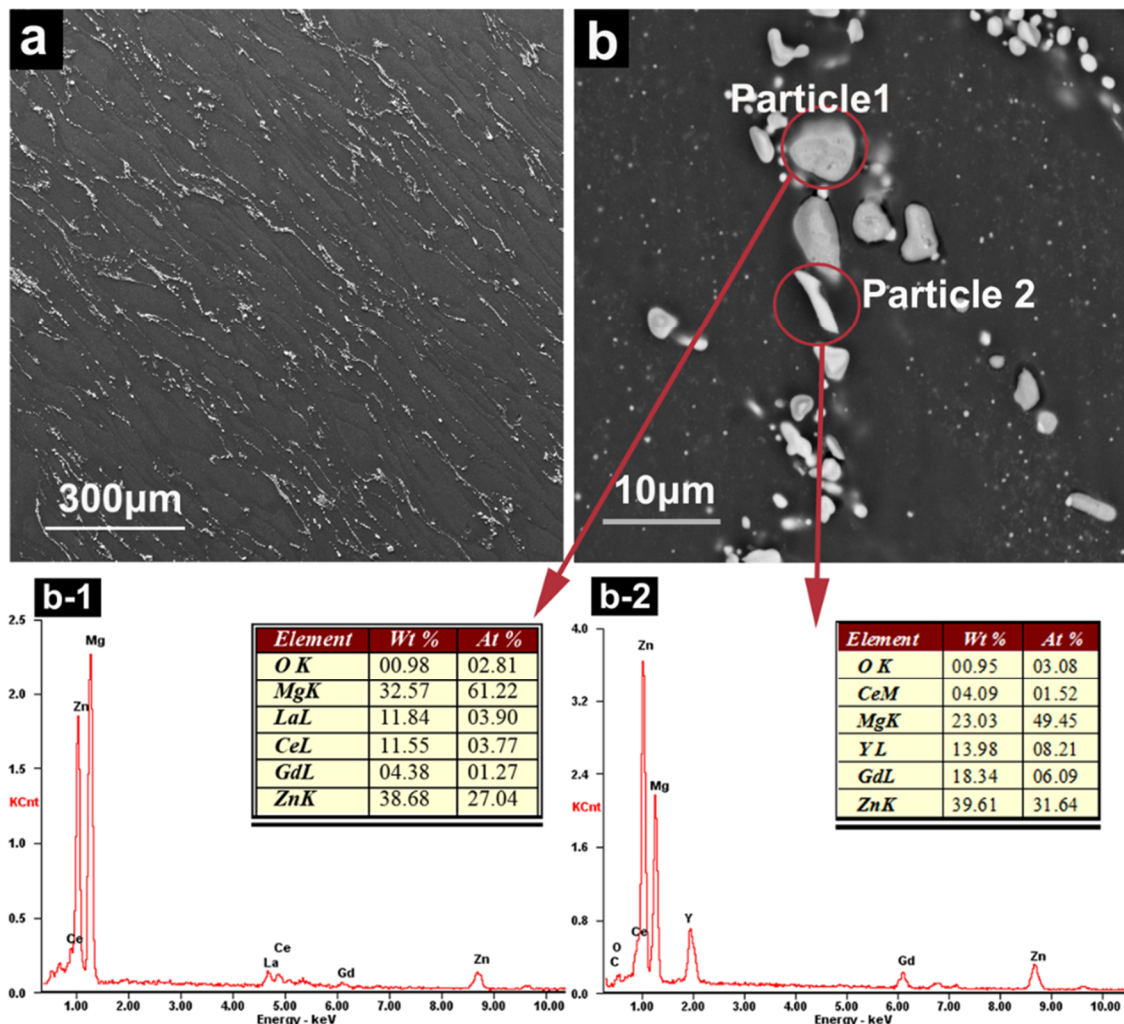
IBM SPSS statistics software 21 was used for statistical analysis. Standard analyses comparing more than two conditions were conducted using a one-way analysis of variance (ANOVA) with Turkey's post hoc test. Statistical values are indicated at the relevant experiments.

### 3. Results

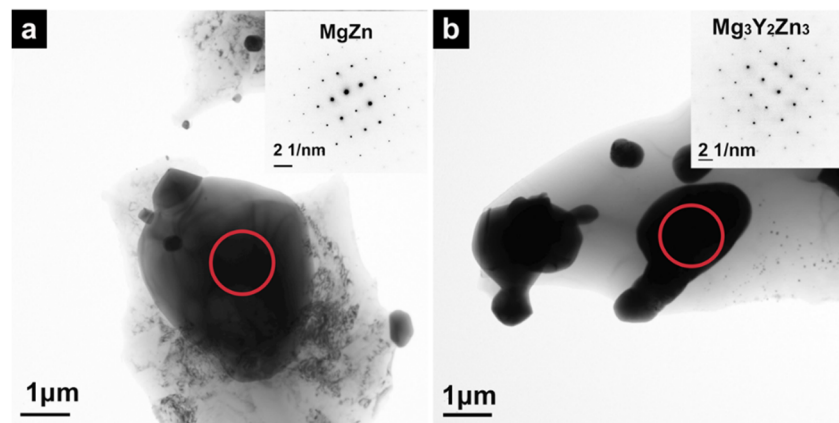
#### 3.1. Precipitates of Mg–6Zn–2.7RE Alloy

Figure 2 shows the microstructure and composition of precipitates. The precipitates distributed at the grain boundaries and inner grains of Mg matrix (Figure 2a) and were identified as RE-rich precipitates by EDS analysis. Based on the relative brightness, there are two main types of precipitate in the alloy, denoted as ‘dark’ or ‘bright’ particles depending on their appearance resulting from contrast differences (Particle 1 and Particle 2 in Figure 2b). The darkness particles mainly contain Mg, Zn, La, Ce and Gd (Figure 2b-1), while the brightness particles mainly contain Mg, Zn, Y, Gd and Ce (Figure 2b-2).

In the selected area electron diffraction (SAED) images in Figure 3, the dark particles appear to be mainly  $\gamma$ -phase MgZn (Figure 3a) [29], and the bright particles are W-phase  $Mg_3Y_2Zn_3$  (Figure 3b) [30]. MgZn can coexist with excess Mg in Mg–6Zn alloys, as shown in the Mg–Zn phase diagram [31]. Therefore, we can conclude that Y and Gd are mainly distributed in  $Mg_3Y_2Zn_3$  particles, and that La and Ce are dissolved in MgZn particles.



**Figure 2.** SEM images and composition of Mg–6Zn–2.7RE after light etching. (a) Overall, distribution of the precipitates; (b) detailed view showing two kinds of precipitate; (b-1,b-2) EDS results of the precipitates shown in Figure 2b.



**Figure 3.** TEM images and selected area electron diffraction (SAED) of two kinds of precipitates in Mg-6Zn-2.7RE. (a)  $\gamma$ -phase MgZn; (b) W-phase  $Mg_3Y_2Zn_3$ .

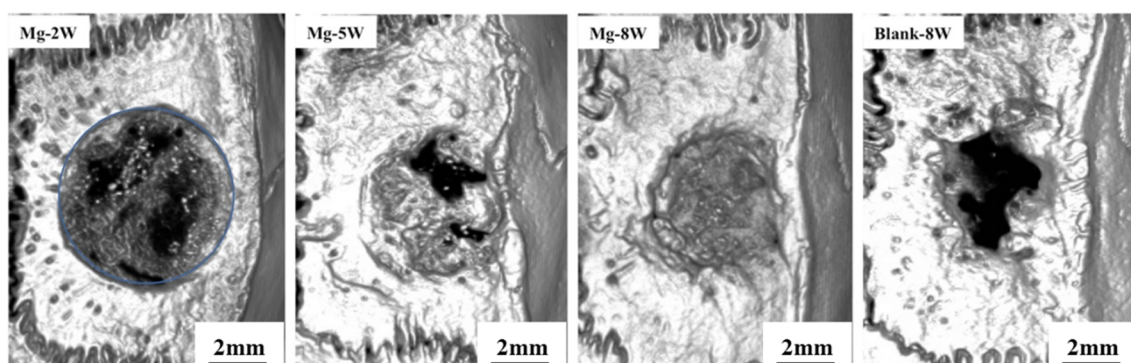
### 3.2. Degradation of Mg-6Zn-2.7RE Alloy and Osteogenesis Processes In Vivo

#### 3.2.1. Clinical Examination

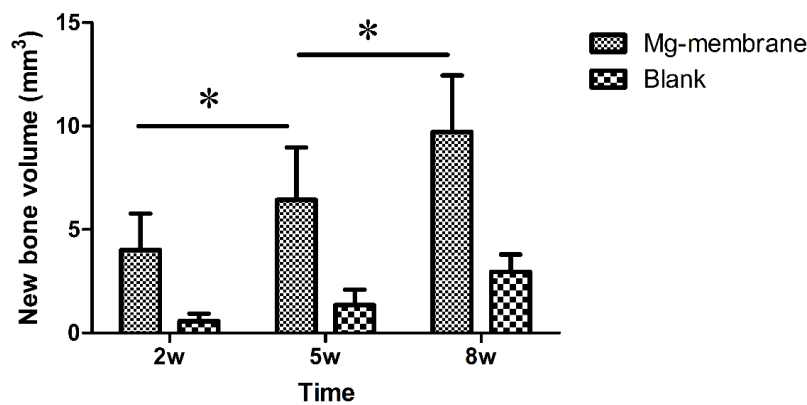
Post-operative wound monitoring revealed swelling, which occurred in most of the animals after 3–7 days and then gradually disappeared within 2 weeks. Despite some initial redness and swelling around the surgical wound, the movement and daily behavior of the tested animals were not affected. No animals died during the observation.

#### 3.2.2. Micro-CT Examination

Figures 4 and 5 show the micro-CT analysis results of rat calvarial defect repair at 2, 5 and 8 weeks after implantation. The Mg-6Zn-2.7RE membrane was degraded into pieces at 2 weeks post-implantation, and the degradation product maintained relative stability throughout the 8-week observation period. New bone formation occurred at the margin and central region of the defect area beneath the Mg alloy membrane in the treated group, while the new bone formation only occurred from the outer margin to the central region in the untreated blank group. Most of the defects were almost totally covered by new bone at 2 weeks post-implantation, and the new bone volume gradually increased and almost completely repaired the whole defect at 5–8 weeks post-implantation in the treated group, while the defects were not completely repaired in the untreated blank group.



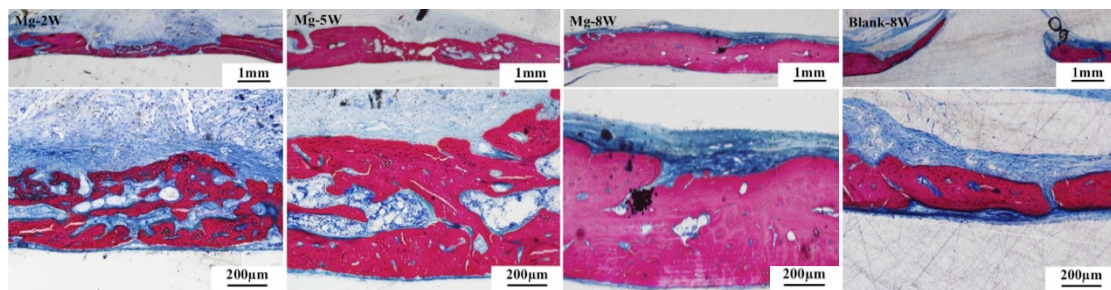
**Figure 4.** Three-dimensional micro-CT photos of rat calvarial defect repair in the treated group after 2, 5 and 8 weeks and in the untreated blank group after 8 weeks of healing. Mg-2W, -5W and -8W: the Mg-6Zn-2.7RE membrane was broken down into pieces at 2, 5- and 8-weeks post-implantation. New bone formation occurred at the margin and central region of the defect area beneath the Mg alloy membrane in the treated group (Mg-2W, Mg-5W, Mg-8W), while new bone formation occurred only between the outer margin and central region in the untreated blank group (Blank-8W).



**Figure 5.** New bone volume in the rat calvarial defects in the treated group after 2, 5 and 8 weeks and the in untreated blank group after 8 weeks of healing as revealed by micro-CT. Most of the defects were almost totally covered by new bone at 2 weeks post-implantation, and the new bone volume gradually increased such that the defect was almost completely repaired at 5–8 weeks post-implantation in the treated group. The defects were not completely repaired in the untreated blank group. \*  $p < 0.01$ .

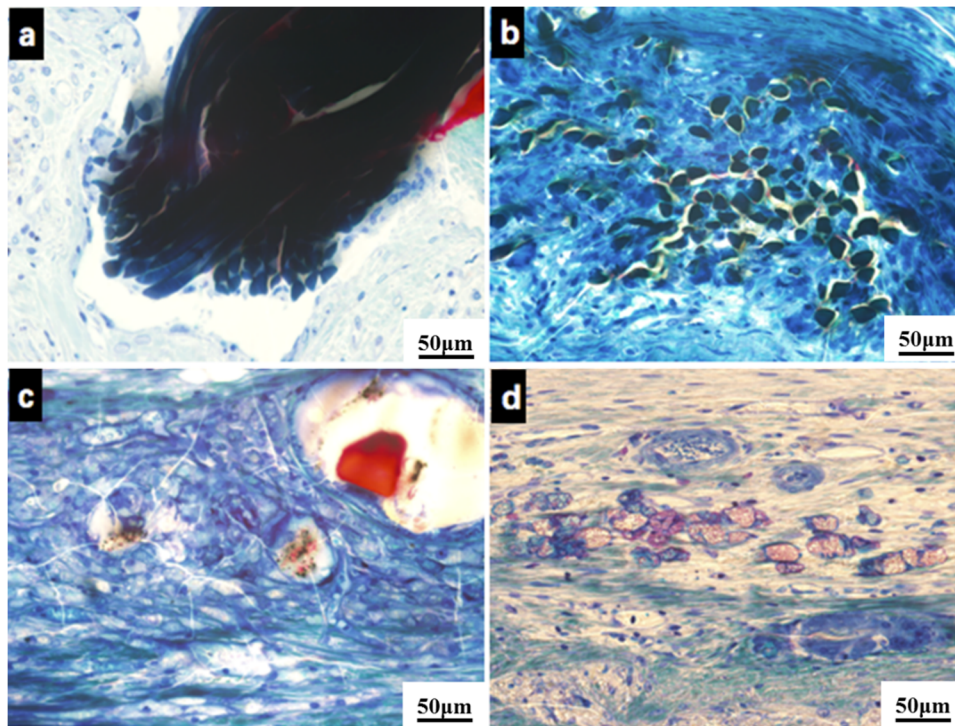
### 3.2.3. Histological Evaluation

Figure 6 shows the tissue response and bone formation progress in the calvarial defect. There are few inflammatory cells in the samples, except for one sample with moderate inflammation. Two weeks after implantation, the newly formed porous bone almost completely covered the bottom of the defect. The margins of the new bone exhibited active osteogenesis, and there was dense pre-mineralized collagen fiber on the surface of the new bone and surface of the holes/cavities within the porous bone material. After 5 and 8 weeks of healing, the new bone thickness and volume had increased further.



**Figure 6.** Histological analysis of bone formation in the treated group after 2, 5 and 8 weeks and in the untreated blank group after 8 weeks. Mg-2 W: at 2 weeks after implantation, the newly formed porous bone almost completely covered the bottom of the defect. Mg-5W, Mg-8W: after 5 and 8 weeks of healing, the thickness and volume of the new bone had further increased.

Figure 7 shows the Mg alloy membrane degradation progress and tissue reaction in vivo. The Mg alloy membrane first degraded into pieces. The pieces further degraded along the grain boundary. Then, the Mg alloy pieces degraded into small particles. Some of the particles were completely degraded and replaced by mineralized collagen tissue, while other particles remained in the tissue.

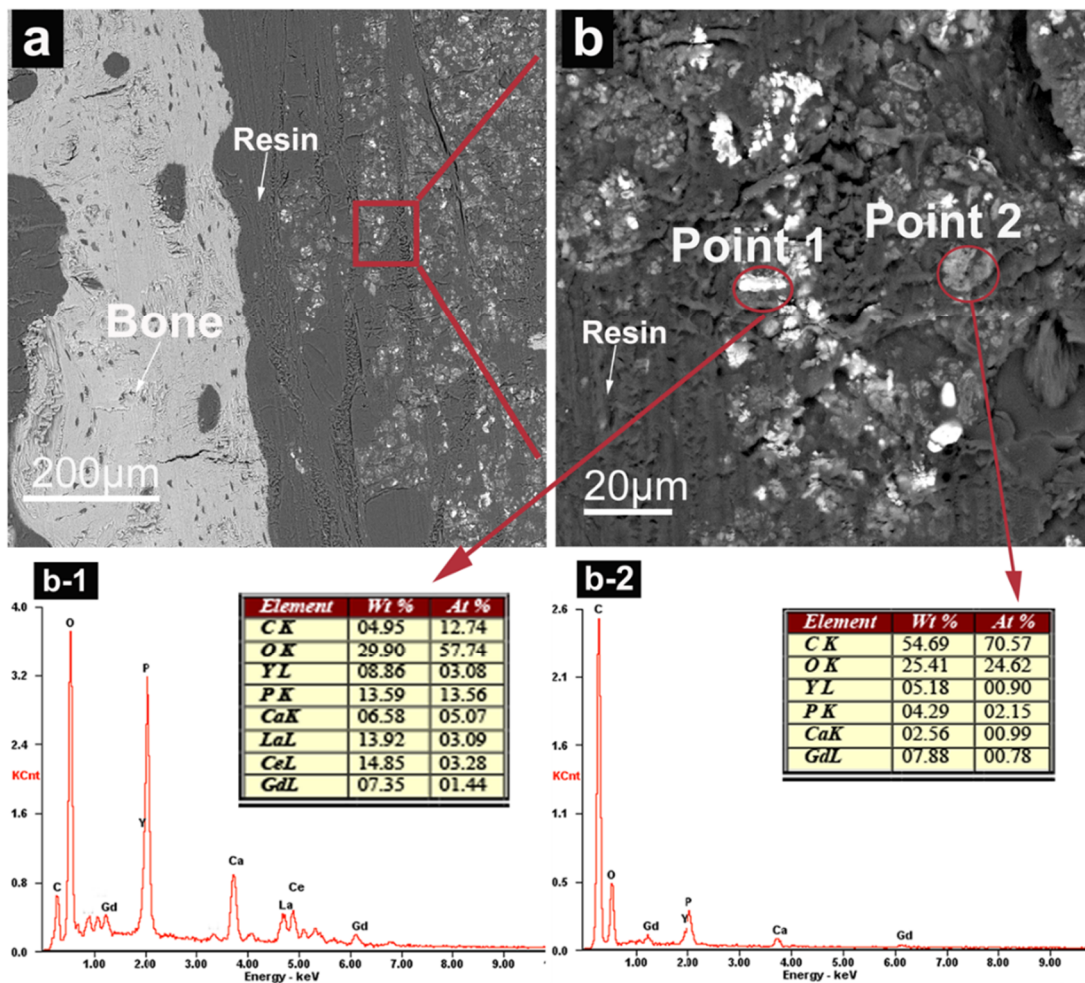


**Figure 7.** Degradation process of the Mg membrane in vivo. (a) Mg alloy membrane first degraded into pieces. (a,b) A gas bubble was produced in the early stage of degradation. Then, the Mg alloy pieces degraded into small particles. (c,d) Some of the particles were completely degraded and replaced by mineralized collagen tissue, while other particles remained in the tissue.

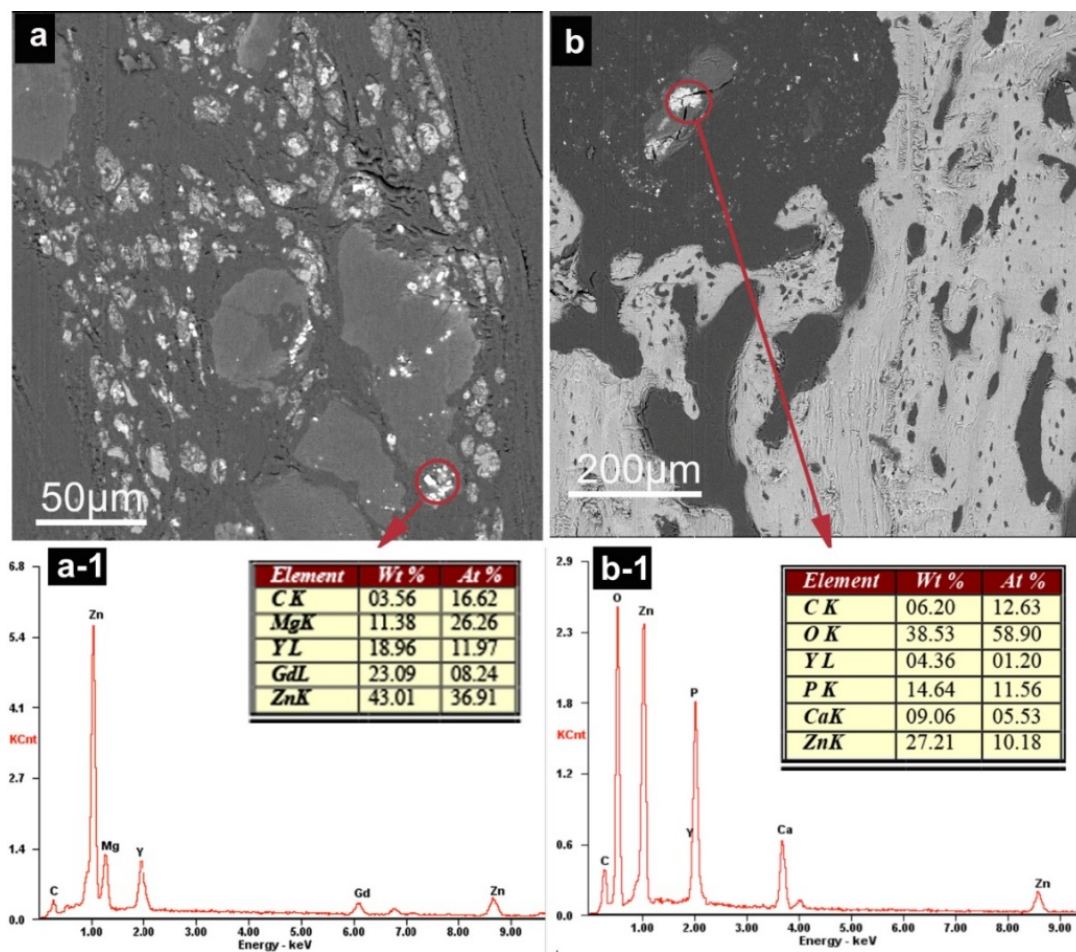
### 3.2.4. SEM Observation and EDS Analysis

Figure 8 shows the SEM results after 8 weeks of degradation in vivo. Most of the degradation products were distributed in the soft tissue and the membrane implantation region. The degradation products can be divided into ‘bright’ particles and ‘dark’ particles; the ‘bright’ particles (Point 1) are composed of a variety of REEs (Y, La, Ce, Gd), P and Ca (Figure 8b, b-1), which likely originated mainly from  $\gamma$ -phase precipitates (Particle 1 in Figure 2); the ‘dark’ particles (Point 2) are composed of Gd, Y, P and Ca (Figure 8b, b-2), which we speculate originated from W-phase precipitates (Particle 2 in Figure 2). In addition, because of the presence of the sprayed C layer and the backing resin, high values of C and O are present in the EDS results.

In addition to the two completely degraded particles in Figure 8, Figure 9 displays some incompletely degraded particles. W-phase particles containing Zn, Mg, Y and Gd still remained in some samples after 5 weeks of degradation (Figure 9a). Figure 9b includes some particles originating from the  $\gamma$ -phase, containing Zn, P, Ca and Y, which remained in samples after 2 weeks of degradation. When particles containing REEs degrade, phosphate forms, as indicated by the P element in Figure 9b.



**Figure 8.** SEM images and energy dispersive spectrometer (EDS) results of the membrane degradation residues after 8 weeks in vivo; (a) SEM images of the membrane degradation residues after 8 weeks; (b) magnified image of the degradation residues; (b-1,b-2) EDS results of the two types of degradation residue particles from Figure 8b.



**Figure 9.** SEM images and EDS results of the membrane degradation residues after 5 and 2 weeks in vivo. (a,b) SEM images of the membrane degradation residues after 5 and 2 weeks, respectively; (a-1,b-1) EDS results of the membrane degradation residues corresponding to Figure 9a,b.

### 3.2.5. Element Concentrations in Organs

The concentrations of Mg, Zn, Gd, Y and La in the adrenal gland, kidney, lung, lymph node, brain, heart, liver and spleen of rats, at 1, 2 and 4 weeks post-implantation of Mg–6Zn–2.7RE alloy membranes, are shown in Figure 10a–e, respectively. The Mg concentration remained stable, except for a slight increase in the adrenal gland and kidney, after 1 week of implantation. Throughout the follow-up period, the concentration of Zn in all the tested organs remained relatively stable, showing no statistically significant difference compared with the negative control. Regarding the concentrations of REEs, Gd showed continuous accumulation in the kidney, liver, lymph node and spleen, Y showed a slight increase in brain and heart after 1 week and La showed continuous accumulation in lymph nodes and liver. The most notable result was that the concentrations of all tested REEs (Gd, Y and La) showed a sharp increase in the lymph node at 4 weeks compared with 1 and 2 weeks. After 4 weeks, the concentrations of Gd, Y and La in the lymph node were  $258.8 \pm 183$  ng/g,  $210.8 \pm 147$  ng/g and  $13.4 \pm 9$  ng/g, respectively. Various REEs are metabolized mainly through lymphatic vessels.

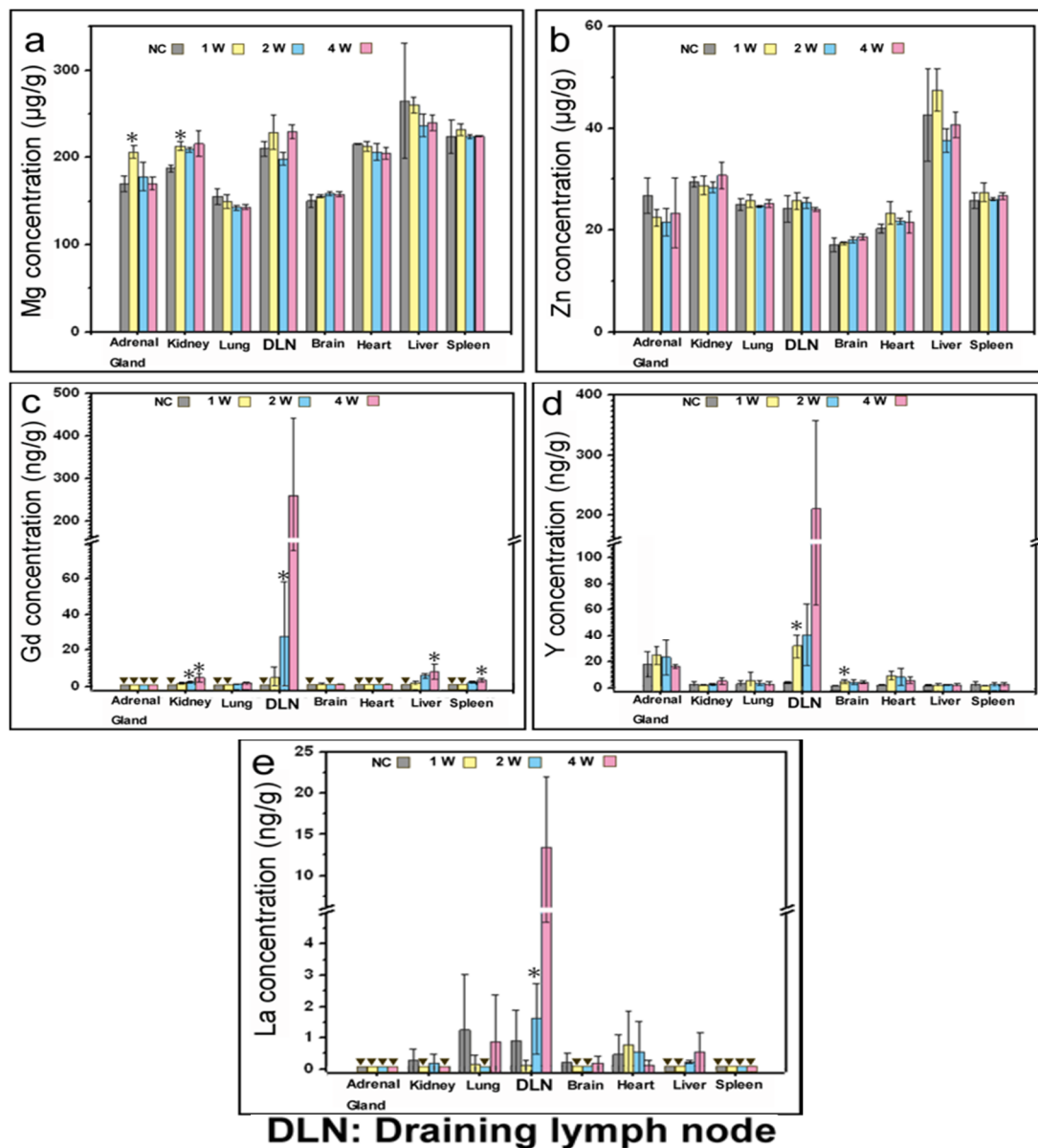


**Figure 10.** The concentrations of (a) Mg, (b) Zn, (c) Gd, (d) Y and (e) La in the adrenal gland, kidney, lung, lymph node (DLN), brain, heart, liver and spleen of rats at 1, 2 and 4 weeks after implantation of Mg–6Zn–2.7RE alloy membranes. The tissues harvested from healthy rats under the same caging and feeding conditions, but without membrane implantation, were considered as the negative control (NC). Note that the mass of the organs was the wet mass. ▼: below the detection limit. \*:  $p < 0.05$ . Test animals:  $n = 5$  for each group (NC, 1W, 2W, 4W).

#### 4. Discussion

For magnesium alloy degradation evaluations, most studies used rat, rabbit [7] or sheep femur or tibia models [32], with a screw or pin implant in the bone, which imitates clinical bone fracture fixation pins. However, there is evidence that Mg alloy has stimulatory effects on the growth of adjacent new bone tissues, so magnesium alloy membrane may be an optimum candidate for guided bone regeneration in dental and craniomaxillofacial bone defects. It is well known from animal models that the geometry of the implant, type of adjacent tissue, buffering capacity and blood flow influence degradation in vivo [33]. Therefore, this study used calvarial defects in rats as an experimental animal model, which has been adopted by many researchers [34,35], to investigate the degradation process and guided bone regeneration capacity of Mg–6Zn–2.7RE membrane.

#### 4.1. Degradation of Mg-6Zn-RE Membrane In Vivo

The Mg-6Zn-2.7RE membrane used in the present study is thin (110  $\mu\text{m}$  thickness), with a large surface area. These characteristics promote rapid degradation and attainment of relative stability within 2 weeks. The degradation process can be divided into two steps: Mg matrix ( $\alpha\text{-Mg}$ ) degradation and precipitate degradation. At the beginning of the degradation process,  $\alpha\text{-Mg}$  acted as an anode, while precipitates acted as a cathode for galvanic corrosion with electrochemical dissolution. As a result, the anodic matrix preferentially degraded due to micro-galvanic corrosion, while the precipitate phase was largely protected. As the degradation continued, some corrosion channels appeared in the  $\alpha\text{-Mg}$  and divided the Mg into debris that degraded independently. At this point, most of the precipitates remained due to cathodic protection [35]. The degradation process vivo in the present study is similar to the in vitro results and models of several other studies [24,35–37].

The second step of the process is precipitate degradation. Along with  $\alpha\text{-Mg}$  degradation, the precipitate phase was partly to completely exposed (Figure 7a). Ion exchange can occur inside the corrosion channels and on the precipitate surface. Temporarily high pH values near the corrosion channel surface during Mg corrosion can lead to the formation of phosphate/carbonate [38], as well as Ca and Mg apatites in the form of  $(\text{Ca}_{1-x}\text{Mg}_x)_{10}(\text{PO}_4)_6\text{OH}_2$  [39]. However, the surface phosphate/carbonate was unstable and dissolution may occur as the cathodic protection of precipitates is reduced due to magnesium matrix dissolution [37]. Therefore, as precipitates are exposed to the physiological environment, the passivation of the Mg, Zn and REEs begins to play a more dominant role. The passive film may consist of  $\text{MgO}$ ,  $\text{Mg}(\text{OH})_2$ ,  $\text{ZnO}$ ,  $\text{RE}_2\text{O}_3$ , etc. The aggressive ions in the physiological environment, such as chloride, destroy the stability of the passive film. Then, metal ions from the destroyed film, together with phosphate, converted into a more stable phosphate compound. The phosphate compound will undergo dissolution at various rates. According to the EDS results of the present study, we speculate that the degradation of precipitates occurs according to the following process. The Mg in precipitates disappears first and Zn and REE remain. These elements may exist mainly in the form of phosphate ( $\text{REPO}_4$ ,  $\text{Ca}_3(\text{PO}_4)_2$  and  $\text{Zn}_3(\text{PO}_4)_2$ ) (Figure 9b). Then,  $\text{Zn}_3(\text{PO}_4)_2$  dissolves, and only a portion of the  $\text{REPO}_4$  and  $\text{Ca}_3(\text{PO}_4)_2$  remains in particles at the original position; the content of REEs and Ca decreases over time (Figure 8). It can be expected that particles rich in REEs in their original position will disappear. Indeed, some particles were completely dissolved, as can be seen in the tissue staining sample (Figure 7), where some red staining, deduced to be from Ca phosphate or apatites, was left in the original position. A schematic of the degradation process is shown in Figure 11.

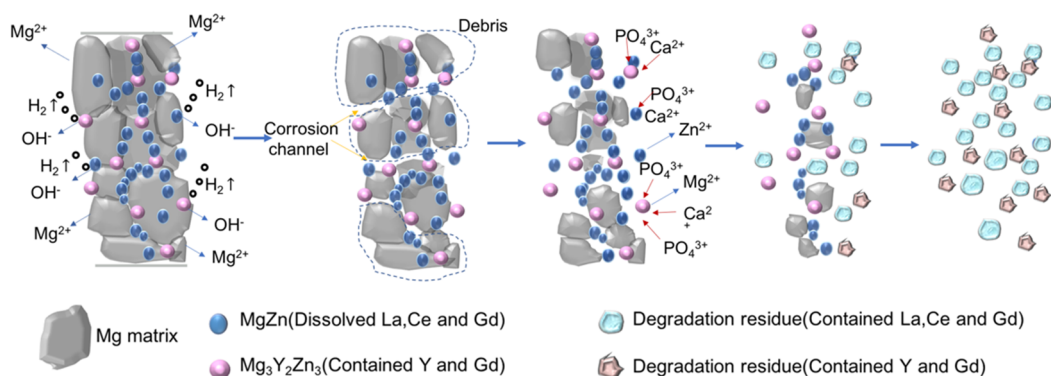


**Figure 11.** A schematic of the degradation process of the Mg-6Zn-2.7RE membrane in vivo.

Two types of particle remained after degradation in vivo, where these correspond to two precipitation phases in the material (although there is a slight difference in the composition of precipitation particles in the material and degraded samples). For example, Point 1 (Figure 8) contains Y element, while Particle 1 (Figure 2) does not, which may be attributable to the large measurement area of Point 1. Therefore, although REEs were added to the alloy, they were not released simultaneously to

the Mg or in proportion to the composition of the alloy. The REE release rate depended on the type and composition of the precipitates. In summary, it is deduced that the degradation process of REEs may be as follows. (1) The REEs in solid solution will be released simultaneously with Mg matrix corrosion; however, it is unknown whether they will form precipitate during the formation of phosphate or carbonate. (2) The REEs in the intermetallic phase will remain stable in the early degradation stage and may then mainly form REPO<sub>4</sub> precipitate and gradually be released in vivo. The release rate depends on the type and composition of the precipitation. Although some studies show that implanted metal particles may lead to inflammation and even osteolysis [23,40], the degradation products and debris of REEs particles showed good biocompatibility without inflammatory reactions in the present study.

#### 4.2. Analysis of Mg, Zn and REES in Organs

Some in vivo studies have used degradable Mg-alloys containing rare earth elements to study the distribution of rare earth elements in many organs and serum samples of animal models [25,26]. However, there are few reports on the transport mechanism of rare earth elements in organs.

Considering that the Mg membrane used in the present study almost completely disintegrated after 2 weeks of implantation, three observation periods (1, 2 and 4 weeks) were chosen to examine the accumulation of elements in organs. We monitored the concentrations of Mg, Zn and REEs in different organs and in lymph nodes, at different time points during degradation of the Mg–6Zn–2.7RE membrane. As a result, we found that the Mg concentration increased slightly in the kidney and adrenal gland after 1 week of implantation, which implied that the Mg mainly moved through the kidneys. These results are consistent with the fact that Mg is excreted in the final urine [41]. The distribution in adrenal glands is consistent with data published in other studies, although the chemical form and route of administration of magnesium may be different [42]. During the degradation of magnesium alloy, the content of magnesium remains stable, which may indicate that magnesium can maintain a relative balance in vivo.

In addition to Mg, Zn is an essential nutrient that plays an important role in the functioning of the human body. In this study, Zn did not accumulate in any of the investigated organs or in the lymph nodes. These results are consistent with those of Zhang et al., who found no significant differences in the Zn levels of six organs (spleen, kidney, liver, heart, lung and brain) between the control and treatment group at the last time point of 20 months [25].

For the more hazardous REEs, toxicity depends on the release rate and systemic accumulation in the body. Although most previous studies showed that REEs did not induce local toxicity or show systemic accumulation [23–25], concerns about the potential for “burst release” of REEs from Mg–RE alloys remain, especially with rapid degradation of the alloy [25]. A burst release-related increase of the elemental concentration of REEs was observed in lymph nodes of the Mg–6Zn–2.7RE-treated group in the present 4-week study. It can be speculated that REEs are mainly transported to the lymphatic system via cell/protein migration or by macrophage uptake. Inhaled or intratracheally instilled RE chlorides have been shown to accumulate in tissue macrophages. In macrophages, REEs were shown to localize in lysosomes and it was proposed that REEs change into insoluble phosphates in lysosomes according to the Gomori (phosphatase) reaction [43]. However, in this study, that REEs may have been engulfed by macrophages after forming rare earth phosphate, and then metabolized through the lymph system. It is worth noting that lymph circulation may be an important route for the REE metabolism. The concentration of REEs shows continuous accumulation in the submandibular lymph node within 2 weeks, which may be attributable to the release of REEs in solid solution associated with Mg matrix degradation. Due to the limited solid solubility of REEs, the concentration thereof in lymph nodes did not show a large increase. After 2 weeks, the precipitate phases rich in REEs were exposed and degraded, which induced a release-related increase in the REE concentration in lymph nodes. Therefore, attention should be given to the burst release of REEs during Mg–RE alloy degradation, which may induce adverse reactions in some organs, such as lymphadenitis. However, we only measured the concentrations of REEs in organs within a 4-week period in the present study. Longer

evaluation periods are needed in future studies. There may be different degradation mechanisms or tissue responses of Mg-based alloys in different shapes and physiological environments. The present study is to investigate the performance of Mg-based alloy membranes in cranio-maxillofacial bone defects which imitates the clinic usage situation for guiding bone regeneration.

#### 4.3. Mg Alloy Membrane-Guided Bone Regeneration

In the field of craniofacial surgery, there are few published animal studies reporting the use of Mg-based materials to guide bone regeneration. Naujokat et al. [33] investigated plates and screws made of Mg for osteosynthesis in a cranio-osteoplasty model in miniature pig and found that the bone healing of the osteoplasty was undisturbed during the entire observation period. Schaller et al. [44] found similar results to Naujokat's using a WE43 plate/screw system on the frontal bone of miniature pigs. The Mg-membranes used in the present study showed excellent osteoconductivity and enhanced bone formation in the vicinity of the implants. This result is consistent with previous reports [22,23,45,46]. Chaya et al. [47] reported that there was enhanced bone formation around a pure Mg plate/screw system in a rabbit ulna fracture model. In our study, the new bone formed rapidly and almost completely covered the defect within 2 weeks, which is rarely reported for modern bone guiding materials such as collagen membranes [40]. An elevated concentration of Mg ions around the implant, in combination with an increase in local pH values and Ca and P deposition, may be promoting of bone development processes [9]. While high pH value has some negative effects on the metabolic activities of osteoclasts which are necessary for bone remodeling, the protein content and cell differentiation are less affected [48].

The osteogenetic process differed between the Mg-membrane test group and the blank group. In the early stages of the experiment, there were many osteogenetic sites and bone-island formations beneath the Mg-membrane, but no continuity. Dense pre-mineralized collagen fiber connected the new bone and then the newly formed bone completely covered the defects. The rapidly formed new bone was porous with many holes and cavities. Active osteogenesis occurred at the surface of the holes/cavities, which were lined with dense pre-mineralized collagen fiber. Then, the bone volume further increased while the porosity decreased (Figure 6). In a previous study, Dziuba et al. [23] inserted a Mg alloy into a bone, and found that the bone volume increased; however, there was a simultaneous reduction in bone density, which may be ascribed to an osteolytic reaction in the early stages and increased osteoclast absorption. In the present study, the bone defect was nearly completely repaired at 8 weeks post-implant. For the blank group, new bone formation occurred from the outer margin to the central region, and the volume of new bone gradually increased during the observation period. The restoration model of the blank group is consistent with modern bone guiding materials, such as collagen membranes and titanium mesh [40]. This study shows promising results for further development of Mg-based membranes for bone-guided regeneration in cranio-maxillofacial surgery. To promote its future clinical application, some kinds of coatings or other surface treatments may be performed to improve the materials' corrosion resistance. Moreover, we have not conducted in vitro experiments on cells since we think the in vitro evaluation may have a certain gap from practical application.

## 5. Conclusions

This study innovatively uses the model as 'critical-sized rat calvarial defects' to analysis the degradation, transportation and osteogenic activity of a REE-containing bioresorbable Mg material (Mg-6Zn-2.7RE). The key results are as follows:

- (1) In the Mg-6Zn-2.7RE membrane degradation process, the Mg matrix degraded first; then, Zn dissolved and REEs were released slowly. The release rate of REEs depended on the type and composition of the precipitates;
- (2) REEs accumulated in draining lymph node, and may be transported mainly through the lymph system;

- (3) The Mg-membrane used in the present study showed excellent biocompatibility and enhanced bone formation in the vicinity of the implants. This result demonstrates that Mg-membranes are a suitable osteoinduction material for cranio-maxillofacial surgery applications.

**Author Contributions:** Conceptualization, J.H. and C.T.; data curation, Y.L.; formal analysis, G.L. and Y.L.; funding acquisition, C.T. and C.G.; methodology, J.W.; project administration, X.Y. and Z.N.; resources, X.Y. and S.Y.; software, M.Z. and Y.L.; validation, G.L. and J.H.; writing—original draft, Y.L.; writing—review & editing, M.Z. and G.L. All authors have read and agreed to the published version of the manuscript.

**Funding:** This research was supported by the National Natural Science Foundation of China (Grant No. 81771119), National Key Research and Development Project (2019YFE0101100) and The Strategic Priority Research of the Chinese Academy of Sciences (XDA16040304).

**Conflicts of Interest:** The authors declare no conflict of interest.

## References

- Li, X.; Liu, X.; Wu, S.; Yeung, K.W.; Zheng, Y.; Chu, P.K. Design of magnesium alloys with controllable degradation for biomedical implants: From bulk to surface. *Acta Biomater.* **2016**, *45*, 2–30. [[CrossRef](#)] [[PubMed](#)]
- Witte, F. Reprint of: The history of biodegradable magnesium implants: A review. *Acta Biomater.* **2015**, *23*, S28–S40. [[CrossRef](#)] [[PubMed](#)]
- Zheng, Y.F.; Gu, X.N.; Witte, F. Biodegradable metals. *Mater. Sci. Eng.* **2014**, *77*, 1–34. [[CrossRef](#)]
- Miao, H.; Zhang, D.; Chen, C.; Zhang, L.; Pei, J.; Su, Y.; Huang, H.; Wang, Z.; Kang, B.; Ding, W.; et al. Research on biodegradable Mg-Zn-Gd alloys for potential orthopedic implants: In vitro and in vivo evaluations. *ACS Biomater. Sci. Eng.* **2019**, *5*, 1623–1634. [[CrossRef](#)]
- Zhao, D.; Wang, T.; Nahan, K.; Guo, X.; Zhang, Z.; Dong, Z.; Chen, S.; Chou, D.T.; Hong, D.; Kumta, P.N.; et al. In vivo characterization of magnesium alloy biodegradation using electrochemical H<sub>2</sub> monitoring, ICP-MS, and XPS. *Acta Biomater.* **2017**, *50*, 556–565. [[CrossRef](#)] [[PubMed](#)]
- Bian, D.; Zhou, W.; Deng, J.; Liu, Y.; Li, W.; Chu, X.; Xiu, P.; Cai, H.; Kou, Y.; Jiang, B.; et al. Development of magnesium-based biodegradable metals with dietary trace element germanium as orthopaedic implant applications. *Acta Biomater.* **2017**, *64*, 421–436. [[CrossRef](#)] [[PubMed](#)]
- Razavi, M.; Huang, Y. Assessment of magnesium-based biomaterials: From bench to clinic. *Biomater. Sci.* **2019**, *7*, 2241–2263. [[CrossRef](#)]
- Zreiqat, H.; Howlett, C.R.; Zannettino, A.; Evans, P.; Schulze-Tanzil, G.; Knabe, C.; Shakibaei, M. Mechanisms of magnesium stimulated adhesion of osteoblastic cells to commonly used orthopaedic implants. *J. Biomed. Mater. Res.* **2002**, *62*, 175–184. [[CrossRef](#)]
- Revell, P.A.; Damien, E.; Zhang, X.S.; Evans, P.J.; Howlett, C.R. The Effect of Magnesium Ions on Bone Bonding to Hydroxyapatite Coating on Titanium Alloy Implants. *Key Eng. Mater.* **2003**, *254*, 447–450. [[CrossRef](#)]
- Chen, Y.; Xu, Z.; Smith, C.; Sankar, J. Recent advances on the development of magnesium alloys for biodegradable implants. *Acta Biomater.* **2014**, *10*, 4561–4573. [[CrossRef](#)]
- Witte, F.; Kaese, V.; Haferkamp, H.; Switzer, E.; Meyer-Lindenberg, A.; Wirth, C.J.; Windhagen, H. In vivo corrosion of four magnesium alloys and the associated bone response. *Biomaterials* **2005**, *26*, 3557–3563. [[CrossRef](#)] [[PubMed](#)]
- Li, J.; Chen, L.; Zhang, X.; Guan, S. Enhancing biocompatibility and corrosion resistance of biodegradable Mg-Zn-Y-Nd alloy by preparing PDA/HA coating for potential application of cardiovascular biomaterials. *Mater. Sci. Eng.* **2020**, *109*, 110607. [[CrossRef](#)] [[PubMed](#)]
- Gupta, M.; Sharon, N.M.L. *Magnesium, Magnesium Alloys, and Magnesium Composites*; John Wiley & Sons: Hoboken, NJ, USA, 2011; pp. 41–42.
- Trivedi, P.; Nune, K.C.; Misra, R.D.K. Degradation behaviour of magnesium rare earth biomedical alloys. *Mater. Technol.* **2016**, *31*, 726–731. [[CrossRef](#)]
- Gusieva, K.; Davies, C.H.J.; Scully, J.R.; Birbilis, N. Corrosion of magnesium alloys: The role of alloying. *Int. Mater. Rev.* **2015**, *60*, 169–194. [[CrossRef](#)]

16. Leng, Z.; Zhang, J.; Zhang, M.; Liu, X.; Zhan, H.; Wu, R. Microstructure and high mechanical properties of Mg–9RY–4Zn (RY: Y-rich misch metal) alloy with long period stacking ordered phase. *Mater. Sci. Eng. A* **2012**, *540*, 38–45. [[CrossRef](#)]
17. Eggebrecht, H.; Rodermann, J.; Hunold, P.; Schmermund, A.; Bose, D.; Haude, M.; Erbel, R. Images in cardiovascular medicine. Novel magnetic resonance-compatible coronary stent: The absorbable magnesium-alloy stent. *Circulation* **2005**, *112*, 303–304. [[CrossRef](#)]
18. Reifenrath, J.; Angrisani, N.; Erdmann, N.; Lucas, A.; Waizy, H.; Seitz, J.M.; Bondarenko, A.; Meyer-Lindenberg, A. Degrading magnesium screws ZEK100: Biomechanical testing, degradation analysis and soft-tissue biocompatibility in a rabbit model. *Biomed. Mater.* **2013**, *8*, 045012. [[CrossRef](#)]
19. Wolters, L.; Besdo, S.; Angrisani, N.; Wriggers, P.; Hering, B.; Seitz, J.M.; Reifenrath, J. Degradation behaviour of LAE442-based plate-screw-systems in an in vitro bone model. *Mater. Sci. Eng. C* **2015**, *49*, 305–315. [[CrossRef](#)]
20. Rettig, R.; Virtanen, S. Composition of corrosion layers on a magnesium rare-earth alloy in simulated body fluids. *J. Biomed. Mater. Res. A* **2009**, *88A*, 359–369. [[CrossRef](#)]
21. He, W.; Zhang, E.; Yang, K. Effect of Y on the bio-corrosion behavior of extruded Mg–Zn–Mn alloy in Hank’s solution. *Mater. Sci. Eng. C* **2010**, *30*, 167–174. [[CrossRef](#)]
22. Kraus, T.; Fischerauer, S.F.; Hanzi, A.C.; Uggowitz, P.J.; Löffler, J.F.; Weinberg, A.M. Magnesium alloys for temporary implants in osteosynthesis: In vivo studies of their degradation and interaction with bone. *Acta Biomater.* **2012**, *8*, 1230–1238. [[CrossRef](#)] [[PubMed](#)]
23. Dziuba, D.; Meyer-Lindenberg, A.; Seitz, J.M.; Waizy, H.; Angrisani, N.; Reifenrath, J. Long-term In vivo degradation behaviour and biocompatibility of the magnesium alloy ZEK100 for use as a biodegradable bone implant. *Acta Biomater.* **2013**, *9*, 8548–8560. [[CrossRef](#)] [[PubMed](#)]
24. Amerstorfer, F.; Fischerauer, S.F.; Fischer, L.; Eichler, J.; Draxler, J.; Zitek, A.; Meischel, M.; Martinelli, E.; Kraus, T.; Hann, S.; et al. Long-term In vivo degradation behavior and near-implant distribution of resorbed elements for magnesium alloys WZ21 and ZX50. *Acta Biomater.* **2016**, *42*, 440–450. [[CrossRef](#)] [[PubMed](#)]
25. Zhang, J.; Li, H.; Wang, W.; Huang, H.; Pei, J.; Qu, H.; Yuan, G.; Li, Y. The degradation and transport mechanism of a Mg–Nd–Zn–Zr stent in rabbit common carotid artery: A 20-month study. *Acta Biomater.* **2018**, *69*, 372–384. [[CrossRef](#)] [[PubMed](#)]
26. Myrissa, A.; Braeuer, S.; Martinelli, E.; Willumeit-Romer, R.; Goessler, W.; Weinberg, A.M. Gadolinium accumulation in organs of Sprague-Dawley(R) rats after implantation of a biodegradable magnesium-gadolinium alloy. *Acta Biomater.* **2017**, *48*, 521–529. [[CrossRef](#)] [[PubMed](#)]
27. Zhang, S.; Zhang, X.; Zhao, C.; Li, J.; Song, Y.; Xie, C.; Tao, H.; Zhang, Y.; He, Y.; Jiang, Y.; et al. Research on an Mg–Zn alloy as a degradable biomaterial. *Acta Biomater.* **2010**, *6*, 626–640. [[CrossRef](#)] [[PubMed](#)]
28. Li, N.; Zheng, Y. Novel Magnesium Alloys Developed for Biomedical Application A Review. *J. Mater. Sci. Tech.* **2013**, *29*, 489–502. [[CrossRef](#)]
29. Watanabe, H.; Moriwaki, K.; Mukai, T.; Ohsuna, T.; Hiraga, K.; Higashi, K. Materials processing for structural stability in a ZK60 magnesium alloy. *Mater. Trans.* **2003**, *44*, 7. [[CrossRef](#)]
30. Luo, Z.; Song, D.; Zhang, S.; Tang, Y.; Zhao, D. Effect of heat-treatment on the stability of the quasicrystal in a Mg–Zn–Zr–Y alloy. *Mater. Lett.* **1994**, *21*, 85–88. [[CrossRef](#)]
31. Ghosh, P.; Mezbahul-Islam, M.; Medraj, M. Critical assessment and thermodynamic modeling of Mg–Zn, Mg–Sn, Sn–Zn and Mg–Sn–Zn systems. *Calphad* **2012**, *36*, 28–43. [[CrossRef](#)]
32. Rossig, C.; Angrisani, N.; Helmecke, P.; Besdo, S.; Seitz, J.M.; Welke, B.; Fedchenko, N.; Kock, H.; Reifenrath, J. In vivo evaluation of a magnesium-based degradable intramedullary nailing system in a sheep model. *Acta Biomater.* **2015**, *25*, 369–383. [[CrossRef](#)] [[PubMed](#)]
33. Naujokat, H.; Seitz, J.M.; Acil, Y.; Damm, T.; Moller, I.; Gulses, A.; Wiltfang, J. Osteosynthesis of a cranio-osteoplasty with a biodegradable magnesium plate system in miniature pigs. *Acta Biomater.* **2017**, *62*, 434–445. [[CrossRef](#)] [[PubMed](#)]
34. Yang, F.; Yang, D.; Tu, J.; Zheng, Q.; Cai, L.; Wang, L. Strontium enhances osteogenic differentiation of mesenchymal stem cells and In vivo bone formation by activating Wnt/catenin signaling. *Stem Cells* **2011**, *29*, 981–991. [[CrossRef](#)] [[PubMed](#)]
35. Song, G.; Atrens, A.; Dargusch, M. Influence of microstructure on the corrosion of diecast AZ91D. *Corros. Sci.* **1998**, *41*, 249–273. [[CrossRef](#)]

36. Deshpande, K.B. Numerical modeling of micro-galvanic corrosion. *Electrochim. Acta* **2011**, *56*, 1737–1745. [[CrossRef](#)]
37. Walter, R.; Kannan, M.B. A mechanistic in vitro study of the microgalvanic degradation of secondary phase particles in magnesium alloys. *J. Biomed. Mater. Res.* **2015**, *103*, 990–1000. [[CrossRef](#)]
38. Song, G. Control of biodegradation of biocompatible magnesium alloys. *Corros. Sci.* **2007**, *49*, 1696–1701. [[CrossRef](#)]
39. Seitz, J.M.; Eifler, R.; Bach, F.W.; Maier, H.J. Magnesium degradation products: Effects on tissue and human metabolism. *J. Biomed. Mater. Res.* **2014**, *102*, 3744–3753. [[CrossRef](#)]
40. Velard, F.; Braux, J.; Amedee, J.; Laquerriere, P. Inflammatory cell response to calcium phosphate biomaterial particles: An overview. *Acta Biomater.* **2013**, *9*, 4956–4963. [[CrossRef](#)]
41. Quamme, G.; Rouffignac, C. Epithelial magnesium transport and regulation by the kidney. *Front. Biosci.* **2000**, *5*, 694–711. [[CrossRef](#)]
42. Kemp, P.A.; Gardiner, S.M.; March, J.E.; Rubin, P.C.; Bennett, T. Assessment of the effect of endothelin-1 and magnesium sulphate on regional blood flows in conscious rats, by the coloured microsphere reference technique. *Br. J. Pharmacol.* **1999**, *126*, 621–626. [[CrossRef](#)] [[PubMed](#)]
43. Hirano, S.; Suzuki, K.T. Exposure, Metabolism, and Toxicity of Rare Earths and Related Compounds. *Environ. Health Perspect.* **1996**, *104*, 85–95. [[PubMed](#)]
44. Schaller, B.; Saulacic, N.; Imwinkelried, T.; Beck, S.; Liu, E.W.; Gralla, J.; Nakahara, K.; Hofstetter, W.; Iizuka, T. In vivo degradation of magnesium plate/screw osteosynthesis implant systems: Soft and hard tissue response in a calvarial model in miniature pigs. *J. Craniomaxillofac. Surg.* **2016**, *44*, 309–317. [[CrossRef](#)] [[PubMed](#)]
45. Liu, D.; Yang, D.; Li, X.; Hu, S. Mechanical properties, corrosion resistance and biocompatibilities of degradable Mg-RE alloys: A review. *J. Mater. Res. Technol.* **2019**, *8*, 1538–1549. [[CrossRef](#)]
46. Kang, M.H.; Lee, H.M.; Jang, T.; Seong, Y.J.; Kim, H.; Koh, Y.; Song, J.; Jung, H. Biomimetic porous Mg with tunable mechanical properties and biodegradation rates for bone regeneration. *Acta Biomater.* **2019**, *84*, 453–467. [[CrossRef](#)]
47. Chaya, A.; Yoshizawa, S.; Verdelis, K.; Myers, N.; Costello, B.J.; Chou, D.T.; Pal, S.; Maiti, S.; Kumta, P.N.; Sfeir, C. In vivo study of magnesium plate and screw degradation and bone fracture healing. *Acta Biomater.* **2015**, *18*, 262–269. [[CrossRef](#)] [[PubMed](#)]
48. Wu, L.; Luthringer, B.J.C.; Feyerabend, F.; Schilling, A.F.; Willumeit, R. Effects of extracellular magnesium on the differentiation and function of human osteoclasts. *Acta Biomater.* **2014**, *10*, 2843–2854. [[CrossRef](#)]



© 2020 by the authors. Licensee MDPI, Basel, Switzerland. This article is an open access article distributed under the terms and conditions of the Creative Commons Attribution (CC BY) license (<http://creativecommons.org/licenses/by/4.0/>).